I. Remec[1], R. M. Ronningen[2], L. Heilbronn[3]

Benchmarking of Heavy Ion Transport Codes

Abstract

Accurate prediction of radiation fields generated by heavy ion interactions is important in medical applications, space missions, and in designing and operation of rare isotope research facilities. In recent years, several well-established computer codes in widespread use for particle and radiation transport calculations have been equipped with the capability to simulate heavy ion transport and interactions. To assess and validate these capabilities, we performed simulations of a series of benchmark-quality heavy ion experiments with the computer codes FLUKA, MARS15, MCNPX, and PHITS. We focus on the comparisons of secondary neutron production. Results are encouraging; however, further improvements in models and codes and additional benchmarking are required.

KEYWORDS:

Heavy ion, transport, benchmarking, FLUKA, MARS15, MCNPX, PHITS

Notice: This manuscript has been authored by UT-Battelle, LLC, under Contract No. DE-AC05-00OR22725 with the U.S. Department of Energy. The United States Government retains and the publisher, by accepting the article for publication, acknowledges that the United States Government retains a non-exclusive, paid-up, irrevocable, world-wide license to publish or reproduce the published form of this manuscript, or allow others to do so, for United States Government purposes.

[1] Oak Ridge National Laboratory, Oak Ridge, TN 37831-6172, USA
[2] Michigan State University, National Superconductiong Cyclotron Laboratory, East Lancing, MI 48824-1321, USA
[3] The University of Tennessee, 1004 Estabrook Road, Knoxville, TN 37996-2300 , USA

Introduction

Simulations of heavy ion (HI) interactions and predictions of resulting radiation fields are needed in such diverse areas as medicine, space exploration, and construction and operation of facilities for scientific research. In medicine, HI beams are used for radiotherapy, and simulations are needed to optimize the treatment [1]. In space explorations, adequate shielding will be needed to protect astronauts in spacecraft and in habitats on the moon or Mars from galactic cosmic radiation (GCR) and solar energetic particle (SEP) events. While GCR and SEP predominantly consist of protons, heavy ions also contribute and are of particular concern because of their higher ionization rate [2]. In facilities dedicated to scientific research with heavy ions, simulations are necessary to support the design of components, such as production targets and beam stops, and predictions of radiation fields are necessary to support shielding design, to assess lifetime of components due to radiation-induced damage, and to plan operation of facilities. One such facility—the Facility for Rare Isotope Beams (FRIB) [3]—is being designed by Michigan State University and will be established as a U.S. Department of Energy Office of Science User Facility in support of the mission of the Office of Nuclear Physics.

FRIB will deliver an energetic beam of primary ions, ranging from hydrogen (at about 600 MeV/proton) to uranium (at about 200 MeV/nucleon) to a production target where rare isotopes will be produced through the fragmentation process. A specific rare isotope, selected for an experiment, will be separated from other fragments and delivered to the experimental area where the capabilities to perform experiments with fast, stopped, or reaccelerated beams will be available. With a primary beam power of 400 kW, the FRIB (which is projected to be complete around 2020) is expected to be the most intense source of rare isotope beams worldwide. A

sketch of a part of the FRIB showing a fragmentation target and a fragment preseparator is displayed in Fig. 1. The FRIB project requires accurate and reliable simulations of HI transport and is the main reason for this benchmarking effort.

While interactions of energetic HIs with targets generate a host of fragments, we will concentrate on the neutron production. Neutrons are the most penetrating secondary particle produced and as such dictate shielding requirements, which in turn often represent a large part of the facility cost. Except in areas in close proximity to the primary beam, neutrons are also responsible for most of the activation and radiation damage to the materials and components of the facility.

Computer Codes

We selected for benchmarking the codes FLUKA [4], MARS15 [5], PHITS [6], and MCNPX [7], mostly because they are well established and in widespread use for particle and radiation transport calculations, but also because members of our collaboration have ample experience with these codes. Significant characteristics of these codes are briefly outlined in the following paragraphs.

FLUKA treats nucleus–nucleus interactions with the Boltzmann Master Equation (BME) at energies below 0.1 GeV/nucleon, with the Modified Relativistic Quantum Molecular Dynamics (RQMD) model in the energy interval from 0.1 GeV/nucleon to 5 GeV/nucleon, and with the Dual Parton Model (DPMJET-II or DMPJET-III) above 5 GeV/nucleon. Hadron–nucleus interactions below 5 GeV/nucleon are treated with the PreEquilibrium Approach to Nuclear Thermalization (PEANUT) cascade model. The version used in this study was FLUKA 2009-b.

MCNPX uses the Los Alamos Quark-Gluon String Model (LAQGSM, version 03.03) for nucleus–nucleus interactions at energies up to ~1 TeV/nucleon. For interactions of protons,

neutrons, pions, and gamma rays at energies below ~3.5 GeV, the Cascade-Exciton Model (CEM) is recommended. Both LAQGSM and CEM include intranuclear cascade, coalescence, and preequilibrium decay, followed by equilibrium evaporation/fission stage. For projectiles with mass numbers less than 13, the Fermi breakup model is also included. Except where specifically marked otherwise, the results reported here were obtained with MCNPX 2.7D03.

MARS15 uses LAQGSM (version 03.03) for nucleus–nucleus interactions at energies up to ~1 TeV/nucleon. At higher energies, DMPJET-III is used. The CEM model is employed as the default for hadron–nucleus interactions below 5 GeV. Both LAQGSM and CEM have capabilities as described in the paragraph on MCNPX. Version of the code used in this work was MARS15.

PHITS uses the JAERI Quantum Molecular Dynamic (JQMD) model for nucleus–nucleus interactions below 100 GeV/nucleon, followed by the General Evaporation Model (GEM). Hadron–nucleus interactions at energies below 200 GeV are treated with the Jet AA Microscopic Transport Model (JAM) and with JQMD or the Bertini model at energies below ~3.5 GeV followed by GEM. Versions PHITS 2.13 and PHITS 2.14 were used in this work.

All of the above-mentioned codes use evaluated cross sections to perform neutron transport at low energies (below ~20 or 14 MeV) and photon cross-section libraries for gamma-ray transport.

The Experiments

The experiments that we selected for benchmarking were performed at the Heavy Ion Medical Accelerator in Chiba (HIMAC) facility of the National Institute of Radiological Sciences in Japan. Figure 2 shows a general layout of the experimental setup for measurements with thin targets.

Ion beams extracted from the synchrotron had a pulse width between 0.5 s and 1 s. Neutron detectors were located at angles from 5 degrees to 80 degrees with respect to the ion beam direction at distances between ~3 m and 5 m from the center of the target as shown in Fig. 2. Neutron detectors were NE213 liquid scintillators shaped cylindrically and having a 12.7-cm-diameter base and 12.7 cm length. With respect to the target, each neutron detector subtended a solid angle ranging from ~0.5 millisteradians (detector at 5°, 5.06 m) to 1.35 msr (detector at 80°, 3.06 m). Neutron spectra were measured with a time-of-flight technique, and precautions were taken to exclude contributions from charged particles, gamma rays, and background generated by neutrons scattered in the room and components of the experimental setup other than the ion target itself. A similar setup was used for the thick target experiments; however, the detectors were located at different angles with respect to the ion beam direction and at different distances from the target. Details about the experiments can be found in Refs. [8], and [9], which were the main sources of data for this work.

Modeling and Simulations

The models of the experimental setup used in the simulations were quite simple, consisting just of the HI beam target and scoring surfaces or volumes representing the neutron detectors. Because the background corrections were applied to the measurements, there was no need to model the room and the details of the experimental setup. The HI beam was modeled as a monodirectional and monoenergetic "pencil beam." To improve the efficiency of the Monte Carlo simulations, neutron current was not tallied over the actual surface area of the detector but, instead, over larger surfaces of the spherical segments. Figure 3a is a three-dimensional sketch of the "tally surfaces," and Fig. 3b gives the dimensions of the surfaces. "Extending" the tallying surface of the detector into a spherical segment does not introduce any approximations, because

the neutron field has axial symmetry around the direction of the HI beam. However, the intervals of the polar angle covered by spherical segments were larger than the polar angle intervals covered by the detectors. This introduces an approximation: in the simulation the neutron spectrum at any given detector location is averaged over a larger polar angle than the measured spectrum. A simulation with tally surfaces equal to detector surfaces was also performed, and it was found that the effect of this approximation is negligible.

Results

Thin targets results

Thin targets are thin in comparison to the beam range; therefore, ion slowdown in the target is small and interactions occur essentially at the beam energy. The contributions of secondary interactions—for example, interactions of secondary fragments in the target—are also negligible. Thin target experiments allow the determination of double-differential neutron production cross sections. Figures 4–7 show comparisons of measured and calculated double-differential neutron spectra. The spectra at each laboratory angle are offset by factors of 10. Figure 8 compares measured and calculated angular distributions of neutrons, which are obtained by integrating double-differential neutron spectra over energy. The statistical uncertainties of the double-differential cross sections obtained from computer simulations were typically better than 1 % and in a few cases reached a few %. The uncertainties of the measured double-differential cross sections varied considerably; however, they were typically in the 20–30 % range, with larger uncertainties typically observed at the highest and the lowest energies at each angle; details can be found in Refs. [8] and [9].

Thick target results

Thick targets are typically slightly thicker than the HI range. In these targets, HIs slow down and ultimately stop so interactions can occur at any energy from the initial beam energy to the threshold for nuclear interactions. Fragments generated by primary HI beam interactions can also interact and contribute to neutron production. The neutrons produced can themselves interact in the target. Figures 9–13 show comparisons of measured and calculated double-differential thick-target neutron yields. The yields at each laboratory angle are offset by factors of 10. Figures 14 and 15 compare measured and calculated angular distributions of neutron yields from thick targets, which are obtained by integrating double-differential neutron yields over energy. The statistical uncertainties of the double-differential thick-target neutron yields obtained from computer simulations were typically better than 1% and in a few cases reached a few %. The uncertainties of the measured double-differential thick-target neutron yields are likely somewhat larger than those of the double-differential cross sections; some information can be found in Ref. [8].

Discussion

All four codes reproduce the basic characteristics of the double-differential neutron spectra from thin targets reasonably well. The spectra at forward directions (at 5 and 10 degrees) exhibit a pronounced peak at the neutron energies approximately corresponding to the energy-per-nucleon of the HI beam, indicating that they are mostly produced by fragmentation of the HI projectiles. However, the spectra also exhibit a “high-energy tail,” which is particularly important in shielding applications. We observed that MCNPX 2.7B predicted excessive production of high energy neutrons in forward direction (Fig. 6a), and we communicated the findings to the code developers. This anomaly was corrected in later versions of the MCNPX code (Fig. 6b) and the MCNP6 code (Fig. 6c). At larger angles with respect to the HI beam direction, the peak in the

neutron spectrum at the specific energy of the HI beam is less pronounced, and these spectra are mostly dictated by neutron emission during the preequilibrium phase, which produces neutrons with energies from a few MeV to several hundred MeV (depending on the HI beam energy) and evaporation from the residual nuclide that dominates neutron spectra at low energies. In general, simulations agree well with the experiment at larger angles, indicating that preequilibrium and equilibrium processes are adequately modeled. It appears that FLUKA, to some extent, overpredicts neutron production from light beams (see Fig. 5) but is more consistent for heavier projectiles. Angular distributions of neutrons are predicted quite well, as illustrated in Fig. 8.

For thick targets, only results from FLUKA and MCNPX are shown here. FLUKA again shows overprediction of neutrons at all angles for lighter ions (see Fig. 9) but agrees better with measurements for heavier projectiles (Figs. 10 and 11). MCNPX results for thick targets are less consistent with the measurements than the results for thin targets. They show considerable underprediction of neutron production for forward directions (0 and 7.5 degrees) from low energies up to the specific energy of the HI beam, and overprediction at 90 degrees at all energies (Figs. 12 and 13). The comparisons of angular distributions of neutron yields from thick targets (Figs. 14 and 15) support the observations made for double-differential neutron yields.

Conclusions

We performed simulations of a series of benchmark-quality heavy ion experiments with the computer codes FLUKA, MARS15, MCNPX, and PHITS. We focused on the comparisons of secondary neutron production. All of the selected codes reproduce reasonably well the shape of the double-differential neutron spectra from thin targets; however, further development appears to be necessary to achieve consistency over the full range of projectile masses and energies.

Simulations of the double-differential thick-target neutron yields were also in reasonable agreement with experiments. Work on benchmarking continues, and a more comprehensive report will be presented upon completion.

Acknowledgments

The authors wish to acknowledge other members of the Heavy Ion Transport Codes Benchmarking Collaboration who contributed to this paper: **Mikhail Kostin** and **Roger Roberts**, Facility for Rare Isotope Beams (FRIB), Michigan State University East Lansing, MI 48824; **Man Yee Betty Tsang**, National Superconducting Cyclotron Laboratory, Michigan State University, East Lansing, MI 48824; **Josh Marshall**, The University of Tennessee,1004 Estabrook Road, Knoxville, TN 37996-2300; **Tony Gabriel**, 9608 Lyttleton Lane, Scientific Investigation and Development, Knoxville, TN 37922; **Yosuke Iwamoto**, Japan Atomic Energy Agency, Tokai, Naka, Ibaraki, 319-1195 Japan; **Koji Niita**, Research Organization for Information Science and Technology,Tokai, Naka, Ibaraki, 319-1195 Japan.

The results presented here are part of R&D efforts on RIBF capabilities supported by the U.S. Department of Energy under contract DE-FG02-08ER41548.

References

[1] Parodi, K., et al., "The FLUKA code for application of Monte Carlo methods to promote high precision ion beam therapy," *12th International Conference on Nuclear Reaction Mechanisms*, Varenna, Italy, 15–19 June 2009, pp. 509–516; http://cdsweb.cern.ch/record/1238366

[2] *Space Radiation Hazards and the Vision for Space Exploration: Report of a Workshop*, Ad Hoc Committee on the Solar System Radiation Environment and NASA's Vision for Space Exploration: A workshop, National Research Council, ISBN: 0-309-66291-5, 2006; http://www.nap.edu/catalog/11760.html

[3] Facility for Rare Isotope Beams: http://frib.msu.edu/

[4] Battistoni, G., Muraro, S, Sala, P. R., Cerutti, F., Ferrari, A., Roesler, S., Fassò, A., Ranft, J., "The FLUKA code: Description and benchmarking," *Proceedings of the Hadronic Shower Simulation Workshop 2006*, Fermilab, 6–8 September 2006, M. Albrow, R. Raja, Eds., AIP Conference Proceeding 896, 2007, pp. 31–49; Fassò, A., Ferrari, A., Ranft, J., and Sala, P. R., *FLUKA: A Multi-particle Transport Code*, CERN-2005-10, 2005, INFN/TC_05/11, SLAC-R-773; http://www.fluka.org/fluka.php

[5] Mokhov, N. V., *The MARS Code System User's Guide*, Version 13(95), Fermilab-FN-628, 1995; http://www-ap.fnal.gov/MARS/

[6] K. Niita, N. Matsuda, Y. Iwamoto, H. Iwase, T. Sato, H. Nakashima, Y. Sakamoto and L. Sihver, "PHITS: Particle and Heavy Ion Transport Code System", Version 2.23, JAEA-Data/Code 2010-022 (2010); http://phits.jaea.go.jp/

[7] McKinney, G. W., et al., *MCNPX 2.7.X—New Features Being Developed*, LA-UR-09-6788, IEEE/NSS Conference, Orlando, FL, 25–31 October 2009; http://mcnpx.lanl.gov/

[8] Nakamura, T., and Heilbronn, L., *Handbook on Secondary Particle Production and Transport by High-Energy Heavy Ions*, ISBN 981-256-558-2, World Scientific, 2005.

[9] Heilbronn, L., et al., "Secondary Neutron-Production Cross Sections from Heavy-Ion Interactions Between 230 and 600 MeV/Nucleon," *Nuclear Science and Engineering*, 157, 2007, p. 142.

Figure Captions

FIG.1—Sketch of the preferred alternative for the FRIB fragmentation target and fragment preseparator area.

FIG. 2—General layout of the HIMAC experimental setup on beamline SB2 for thin targets measurements.

FIG. 3—Model of the experiment used for simulations with MCNPX code: a) three-dimensional sketch of the surfaces used for tallying neutrons; b) details of the surface dimensions.

FIG. 4—Measured and calculated double-differential neutron spectra from 400 MeV/nucleon ^{132}Xe on 0.9-cm-thick Li target; a) MARS15 simulation; b) MCNPX simulation.

FIG. 5—Measured and calculated double-differential neutron spectra from 230 MeV/nucleon ^{4}He on thin (2.0 cm) Al target: a) PHITS simulation; b) FLUKA simulation.

FIG. 6—Measured and calculated double-differential neutron spectra from 600 MeV/nucleon Si on 0.4-cm-thick Cu target: a) MCNPX2.7B simulation; b) MCNPX 2.7D03 simulation; c) MCNP6 simulation.

FIG. 7—Measured and calculated double-differential neutron spectra from 400 MeV/nucleon ^{132}Xe on 0.05-cm-thick Pb target: a) PHITS simulation; b) MCNPX simulation.

FIG. 8—Angular distribution of neutrons from 400 MeV/nucleon ^{132}Xe on a) 0.9-cm-thick Li target and b) 0.05-cm-thick Pb target. Simulations were performed with the MCNPX code.

FIG. 9—Measured and calculated double-differential thick-target neutron yields from 400 MeV/nucleon C on a 15.0-cm-thick Al target. Simulations were performed with the FLUKA code.

FIG. 10—Measured and calculated double-differential thick-target neutron yields from 400 MeV/nucleon Ar on a 5.5-cm-thick Al target. Simulations were performed with the FLUKA code.

FIG. 11—Measured and calculated double-differential thick-target neutron yields from 400 MeV/nucleon Fe on a 3.0-cm-thick Al target. Simulations were performed with the FLUKA code.

FIG.12—Measured and calculated double-differential thick-target neutron yields from 400 MeV/nucleon C on a 5.0-cm-thick Cu target: a) at laboratory angles 0, 7.5, and 15 degrees; b) at laboratory angles 30, 60, and 90 degrees. Simulations were performed with the MCNPX code.

FIG.13—Measured and calculated double-differential thick-target neutron yields from 400 MeV/nucleon Ar on 5.5-cm-thick Al target: a) at laboratory angles 0, 7.5, and 15 degrees; b) at laboratory angles 30, 60, and 90 degrees. Simulations were performed with the MCNPX code.

FIG. 14—Measured and calculated angular distribution of neutrons from a) 400 MeV/nucleon Ar on 5.5-cm-thick Al target, and b) 400 MeV/nucleon Ne on 8.0-cm-thick Al target. Simulations were performed with the FLUKA code.

FIG. 15—Measured and calculated angular distribution of neutrons from a) 400 MeV/nucleon C on 5.0-cm-thick Cu target, and b) 400 MeV/nucleon Ar on 5.5-cm-thick Al target. Simulations were performed with the MCNPX code.

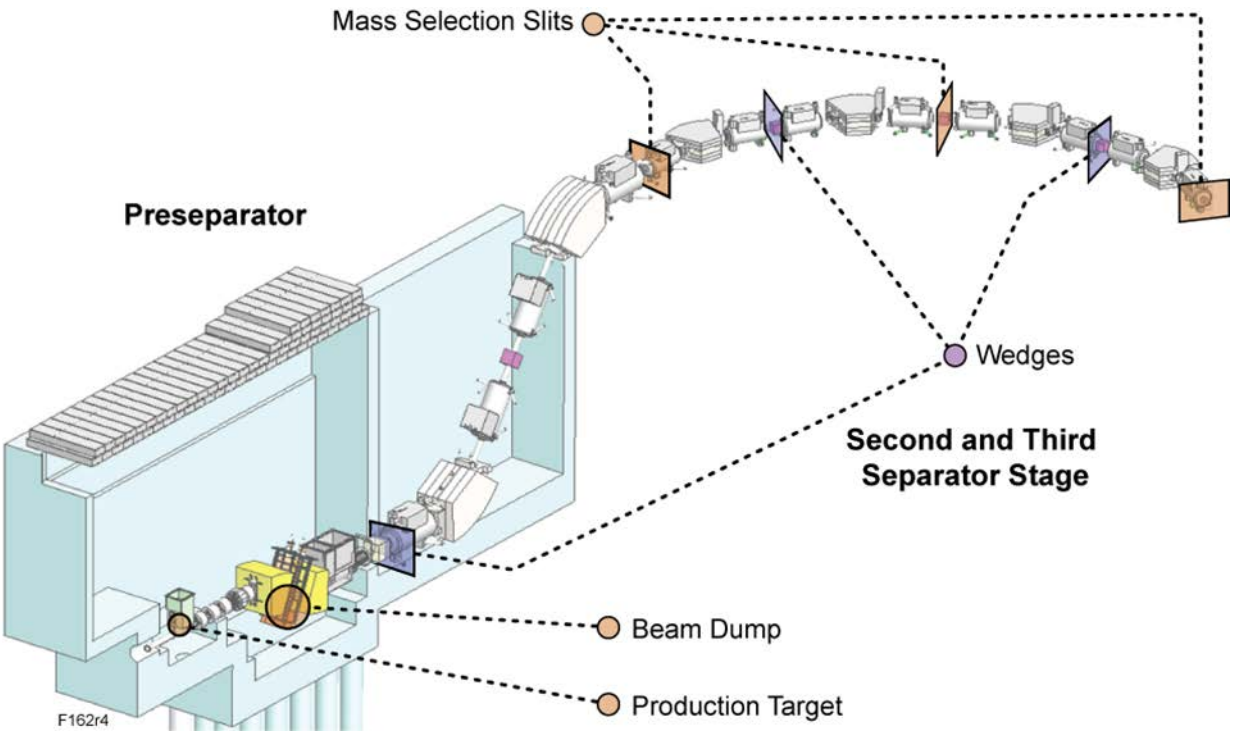

FIG.1—*Sketch of the preferred alternative for the FRIB fragmentation target and fragment preseparator area.*

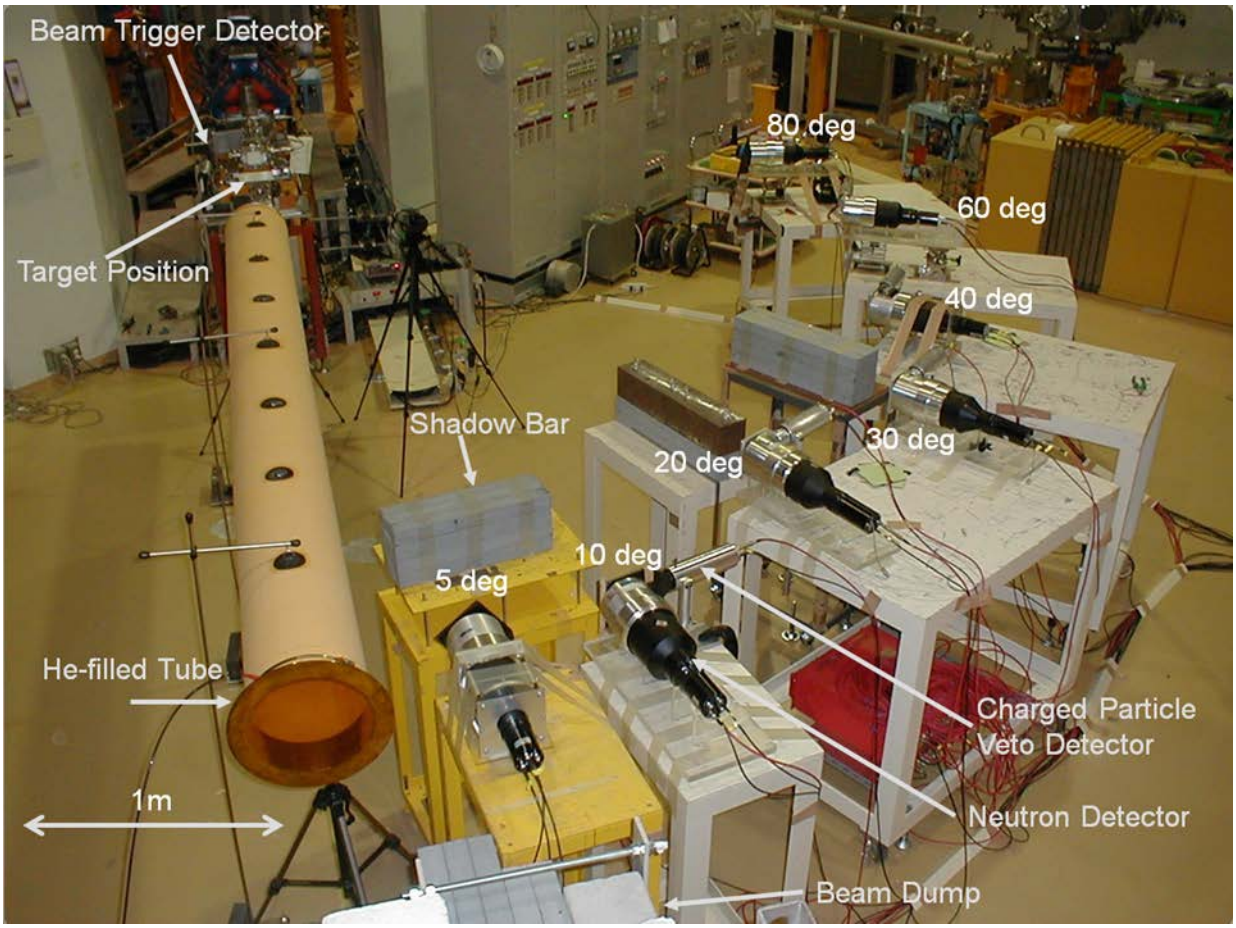

FIG. 2—*General layout of the HIMAC experimental setup on beamline SB2 for thin targets measurements.*

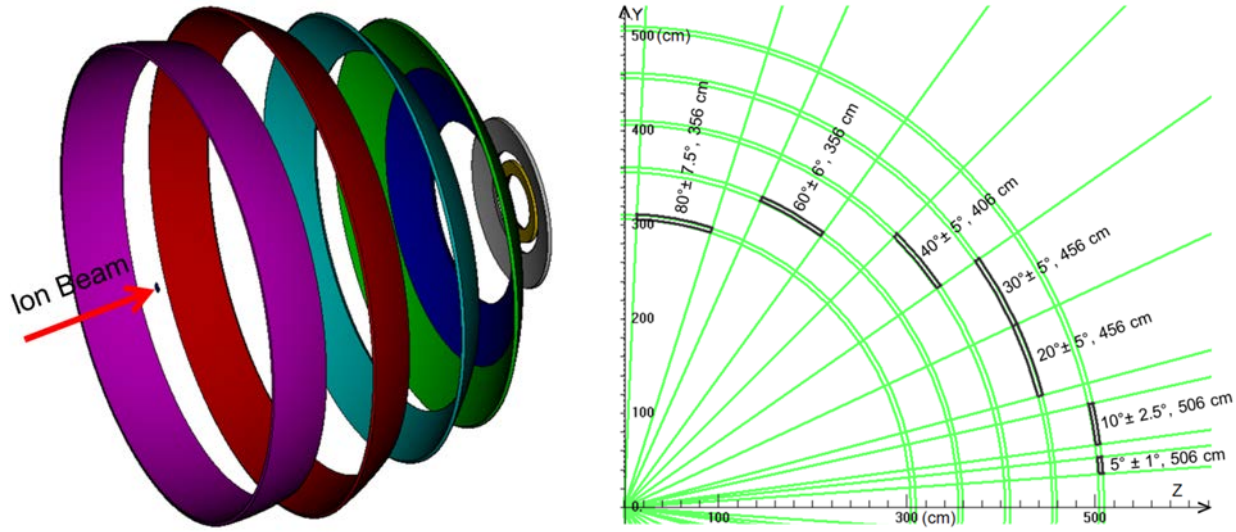

a) b)

FIG. 3—*Model of the experiment used for simulations with MCNPX code: a) three dimensional sketch of the surfaces used for tallying neutrons; b) details of the surface dimensions.*

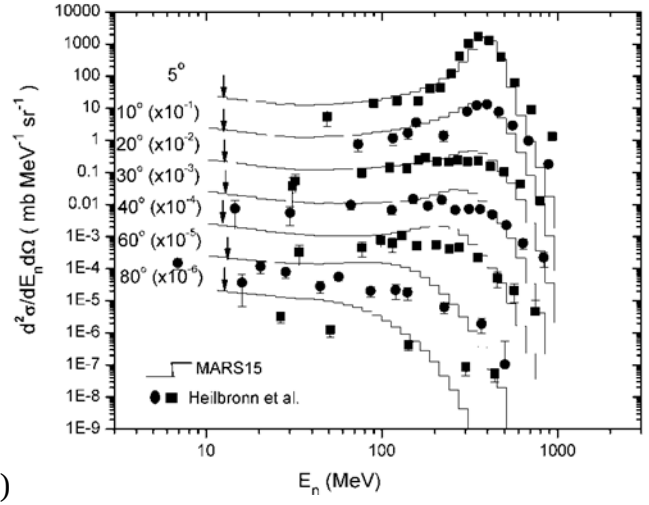

a)

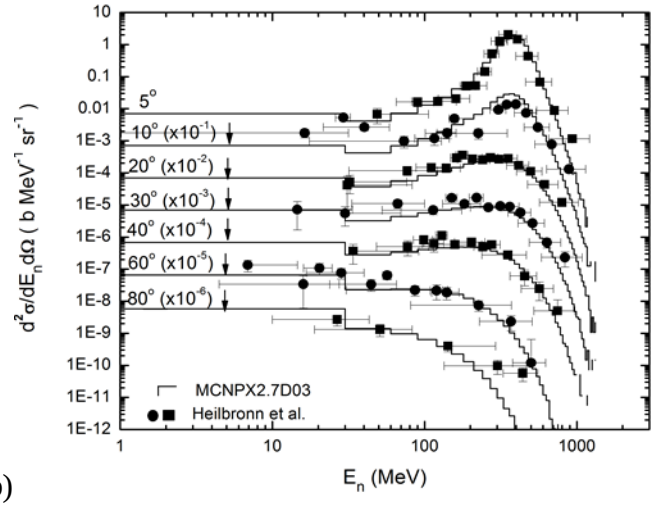

b)

FIG. 4—*Measured and calculated double-differential neutron spectra from 400 MeV/nucleon* ^{132}*Xe on 0.9-cm-thick Li target; a) MARS15 simulation; b) MCNPX simulation.*

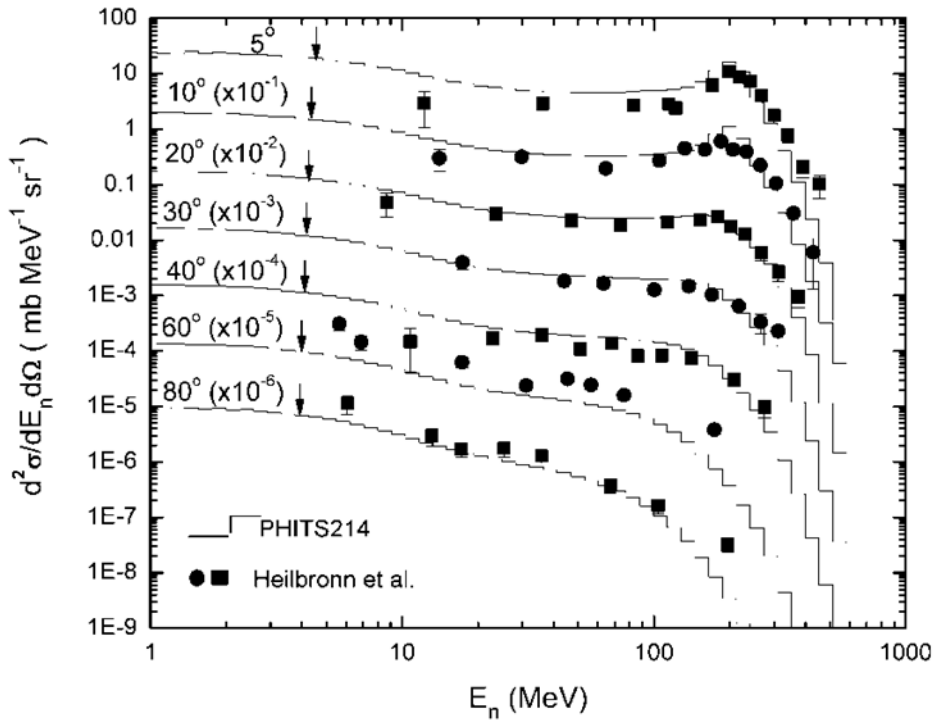

a)

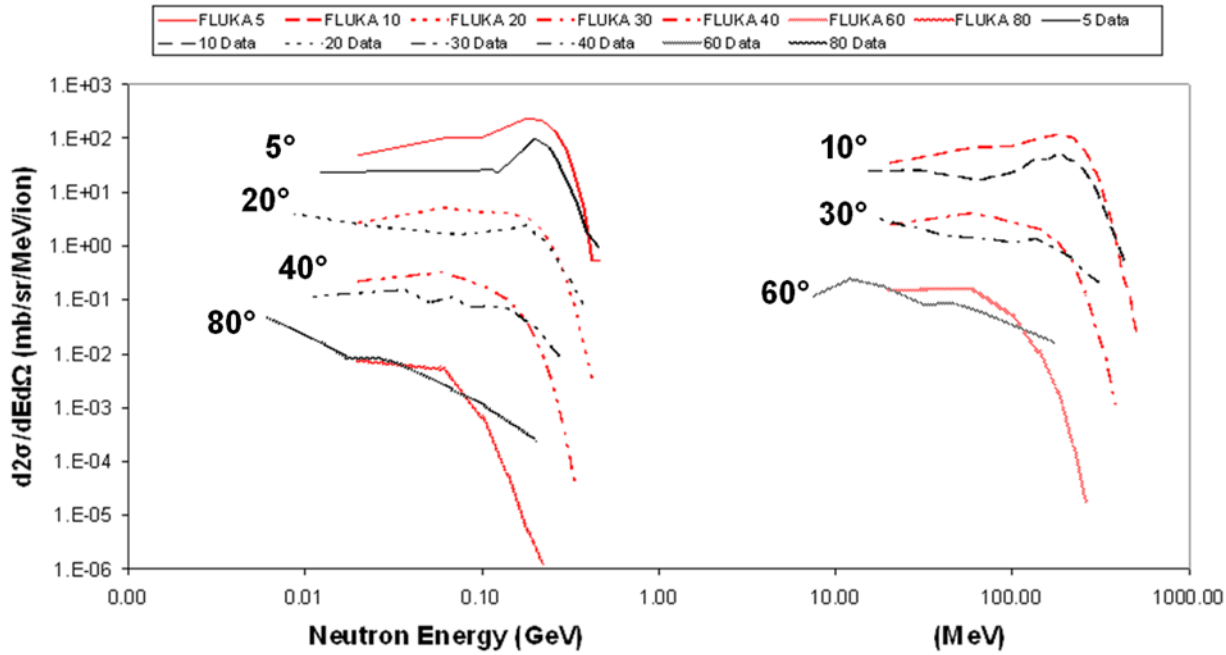

b)

FIG. 5—*Measured and calculated double-differential neutron spectra from 230 MeV/nucleon* ^{4}*He on thin (2.0 cm) Al target: a) PHITS simulation; b) FLUKA simulation.*

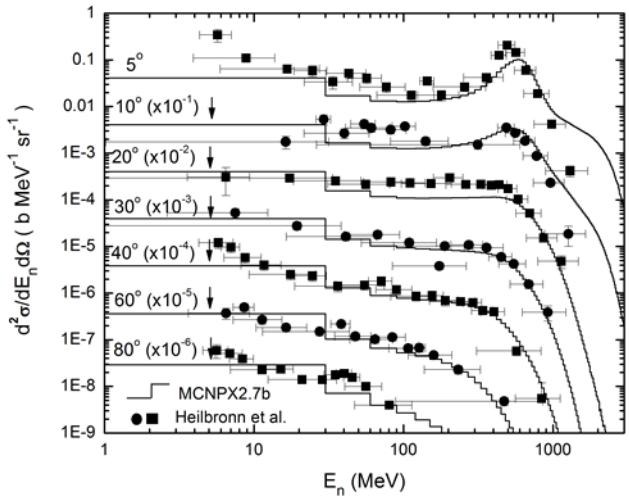

a)

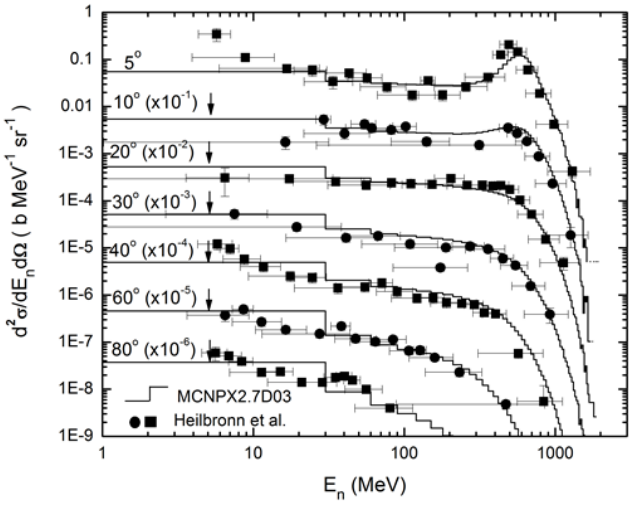

b)

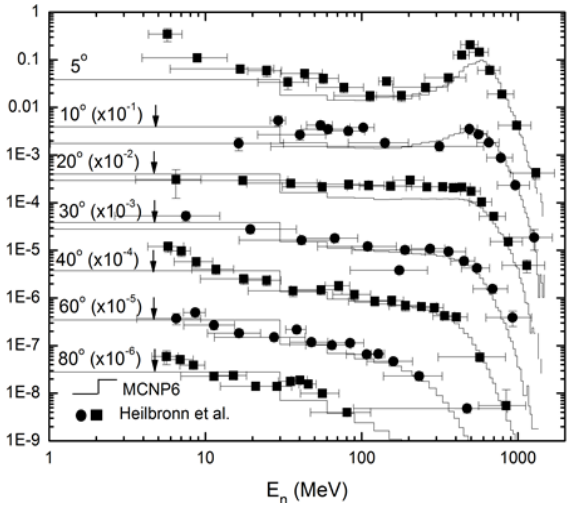

c)

FIG. 6—*Measured and calculated double-differential neutron spectra from 600 MeV/nucleon Si on 0.4-cm-thick Cu target: a) MCNPX2.7B simulation; b) MCNPX 2.7D03 simulation; c) MCNP6 simulation.*

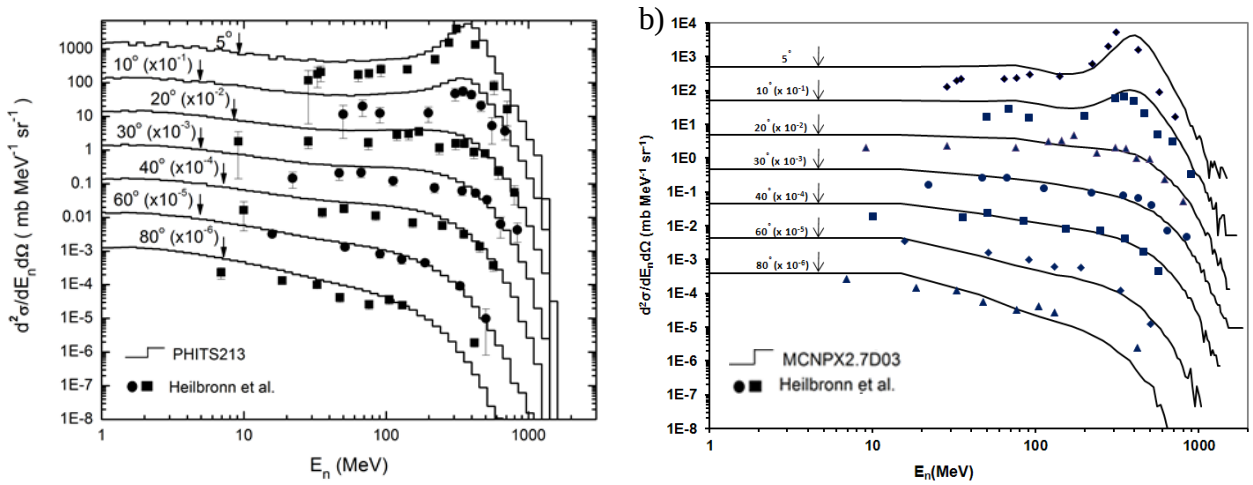

a)

FIG. 7—*Measured and calculated double-differential neutron spectra from 400 MeV/nucleon* ^{132}*Xe on 0.05-cm-thick Pb target: a) PHITS simulation; b) MCNPX simulation.*

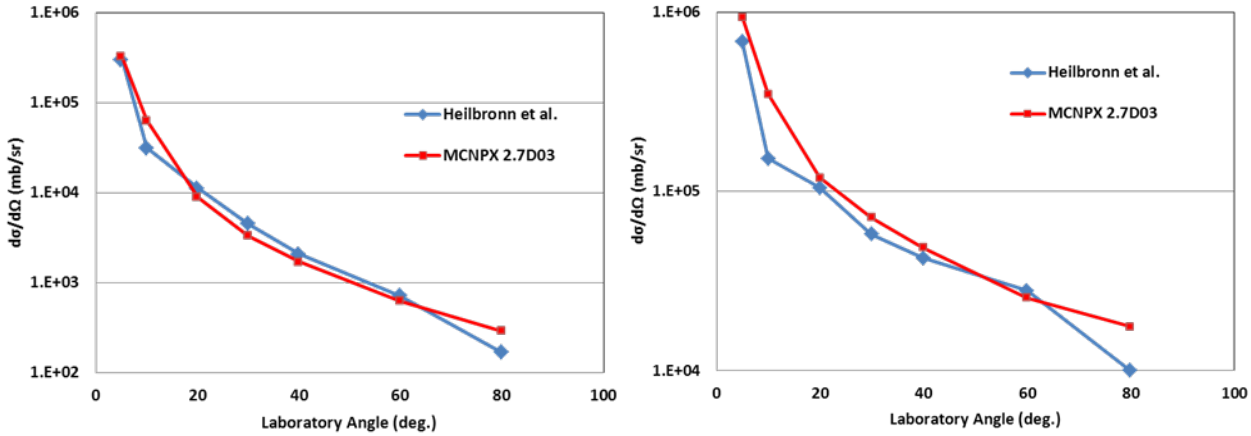

a) b)

FIG. 8—*Angular distribution of neutrons from 400 MeV/nucleon* ^{132}*Xe on a) 0.9-cm-thick Li target and b) 0.05-cm-thick Pb target. Simulations were performed with the MCNPX code.*

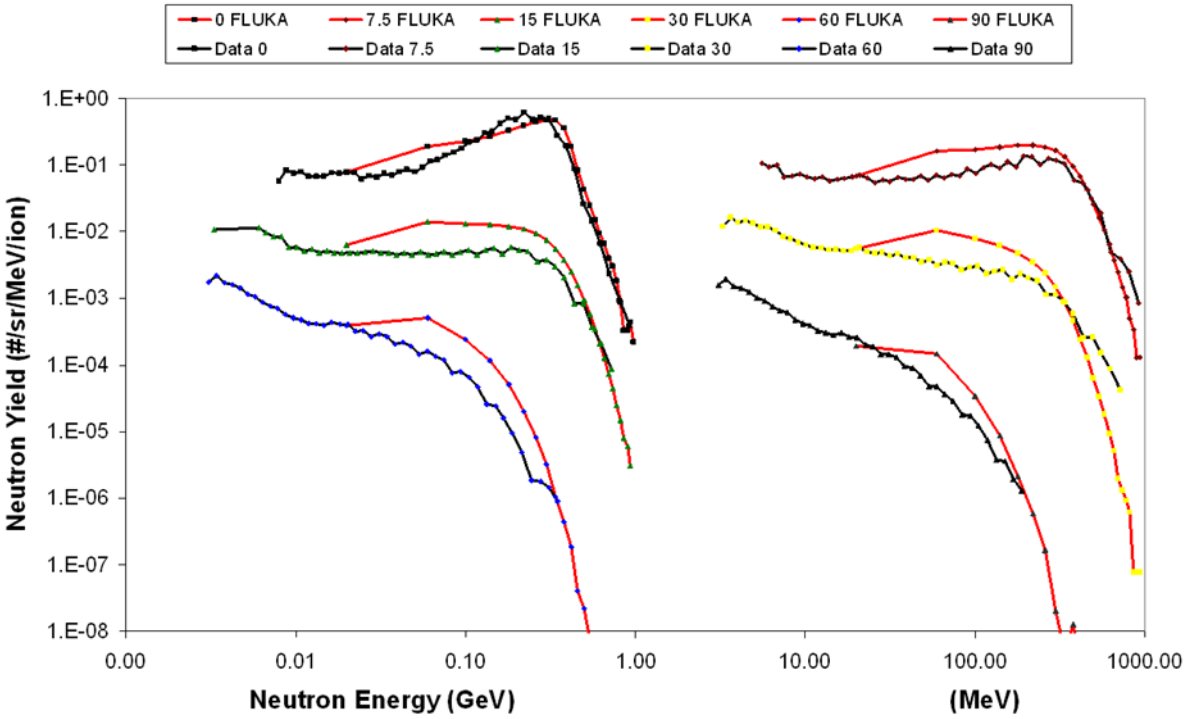

FIG. 9—*Measured and calculated double-differential thick-target neutron yields from 400 MeV/nucleon C on a 15.0-cm-thick Al target. Simulations were performed with the FLUKA code.*

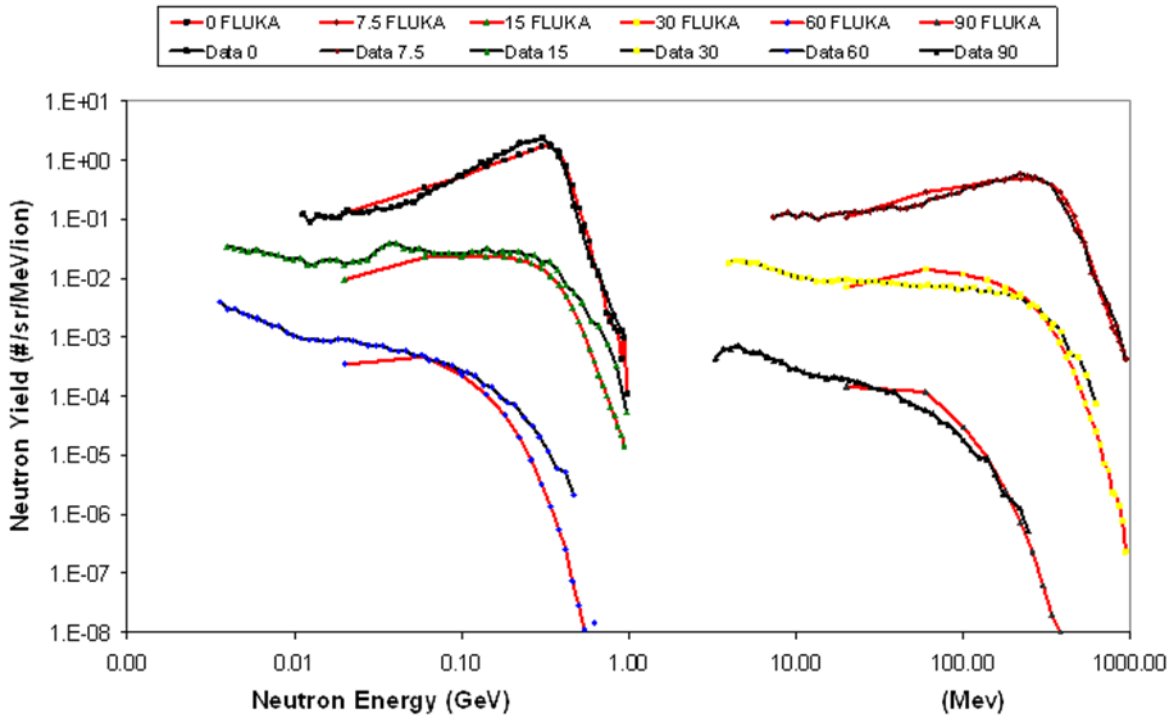

FIG. 10—*Measured and calculated double-differential thick-target neutron yields from 400 MeV/nucleon Ar on a 5.5-cm-thick Al target. Simulations were performed with the FLUKA code.*

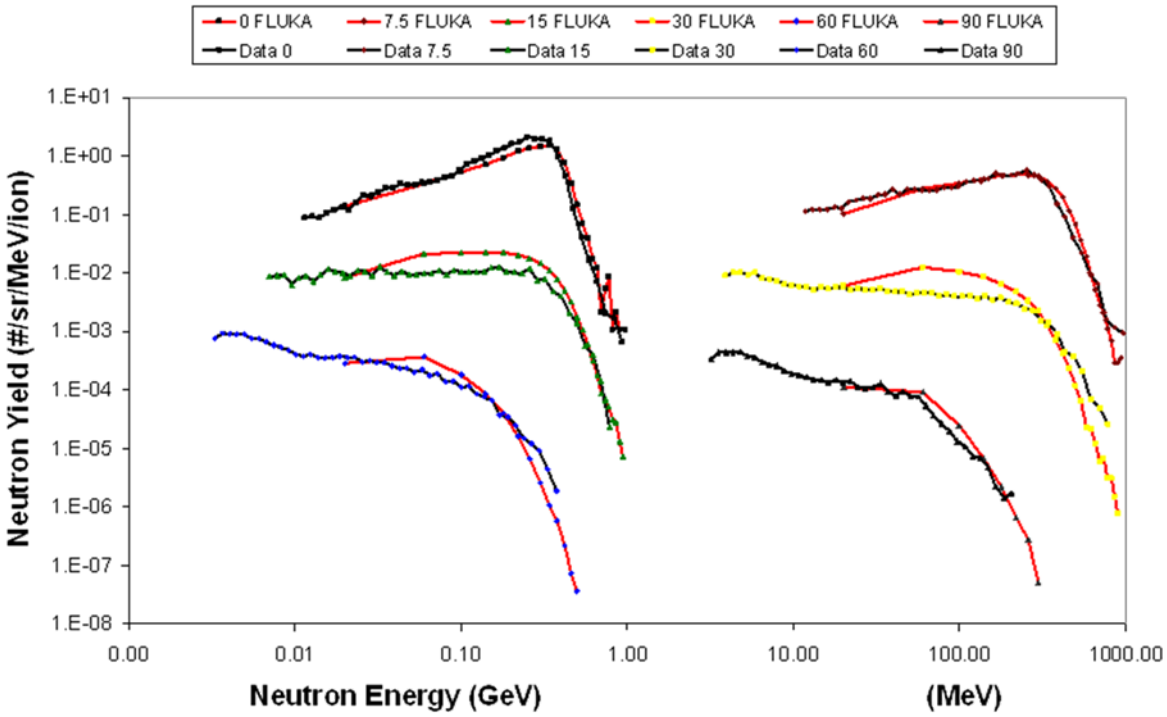

FIG. 11—*Measured and calculated double-differential thick-target neutron yields from 400 MeV/nucleon Fe on a 3.0-cm-thick Al target. Simulations were performed with the FLUKA code.*

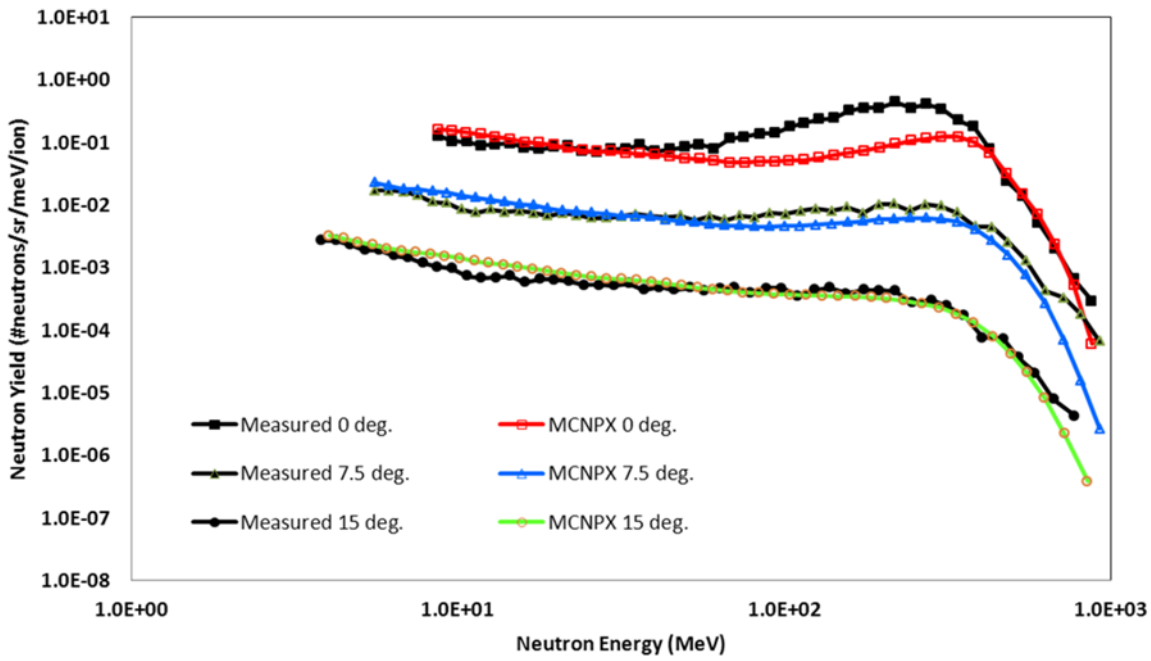

a)

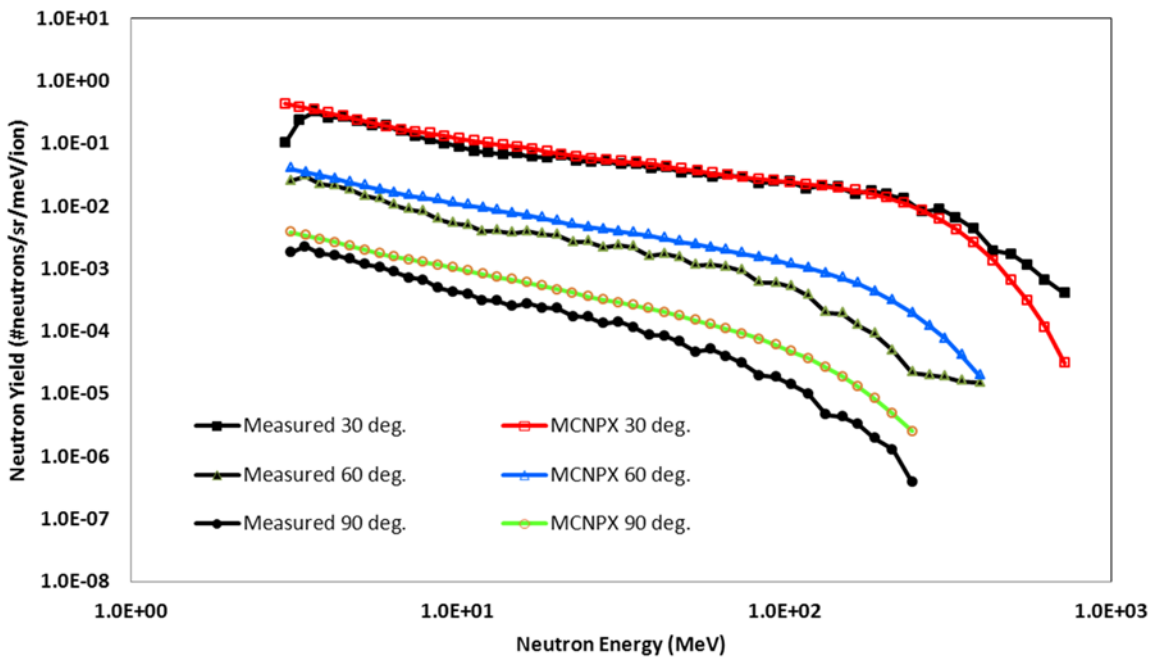

b)

FIG.12—*Measured and calculated double-differential thick-target neutron yields from 400 MeV/nucleon C on a 5.0-cm-thick Cu target: a) at laboratory angles 0, 7.5, and 15 degrees; b) at laboratory angles 30, 60, and 90 degrees. Simulations were performed with the MCNPX code.*

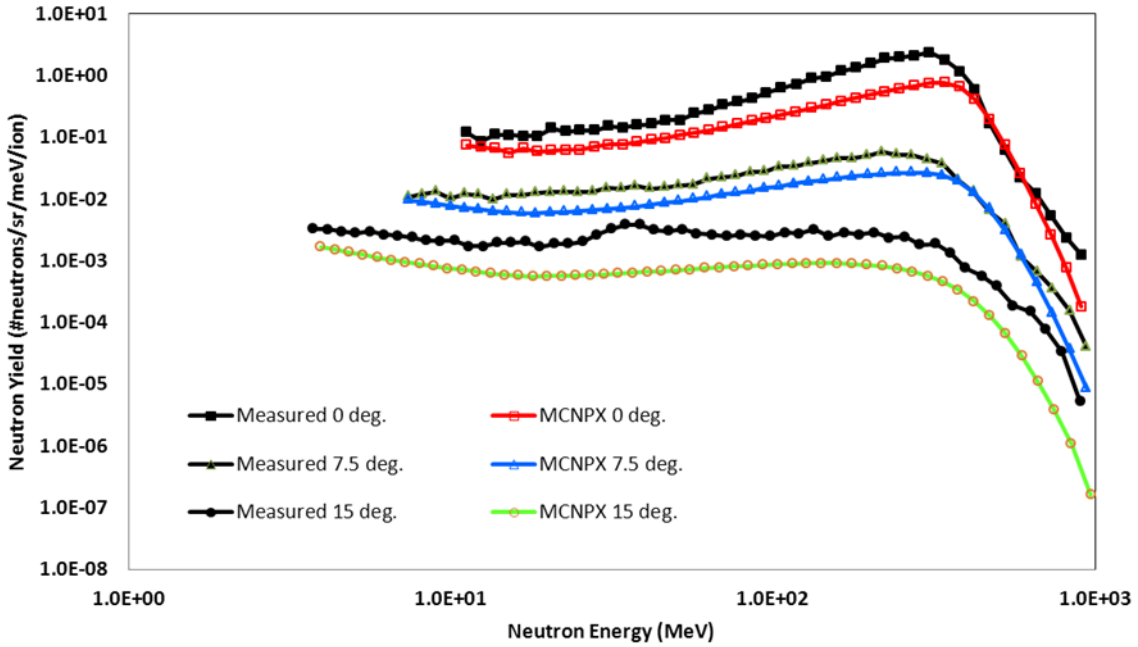

a)

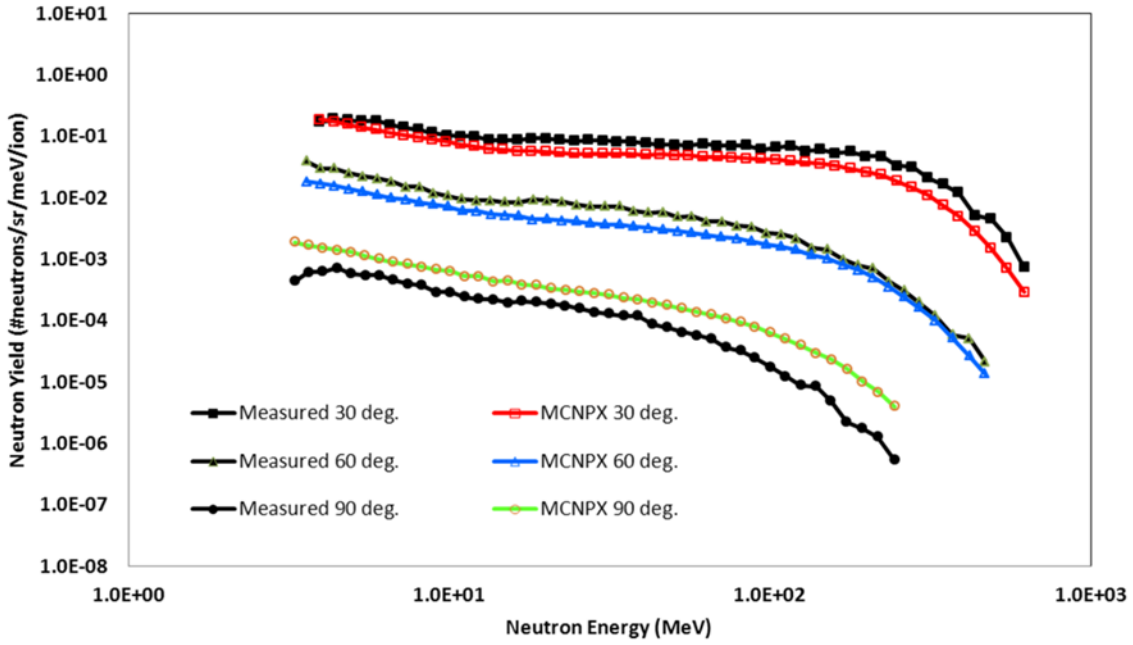

b)

FIG.13—*Measured and calculated double-differential thick-target neutron yields from 400 MeV/nucleon Ar on 5.5-cm-thick Al target: a) at laboratory angles 0, 7.5, and 15 degrees; b) at laboratory angles 30, 60, and 90 degrees. Simulations were performed with the MCNPX code.*

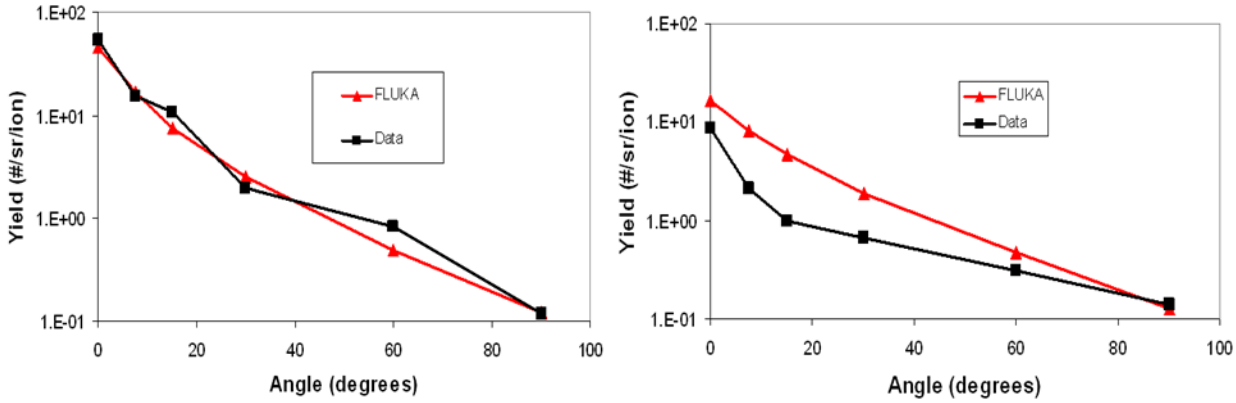

a) b)

FIG. 14—*Measured and calculated angular distribution of neutrons from a) 400 MeV/nucleon Ar on 5.5-cm-thick Al target, and b) 400 MeV/nucleon Ne on 8.0-cm-thick Al target. Simulations were performed with the FLUKA code.*

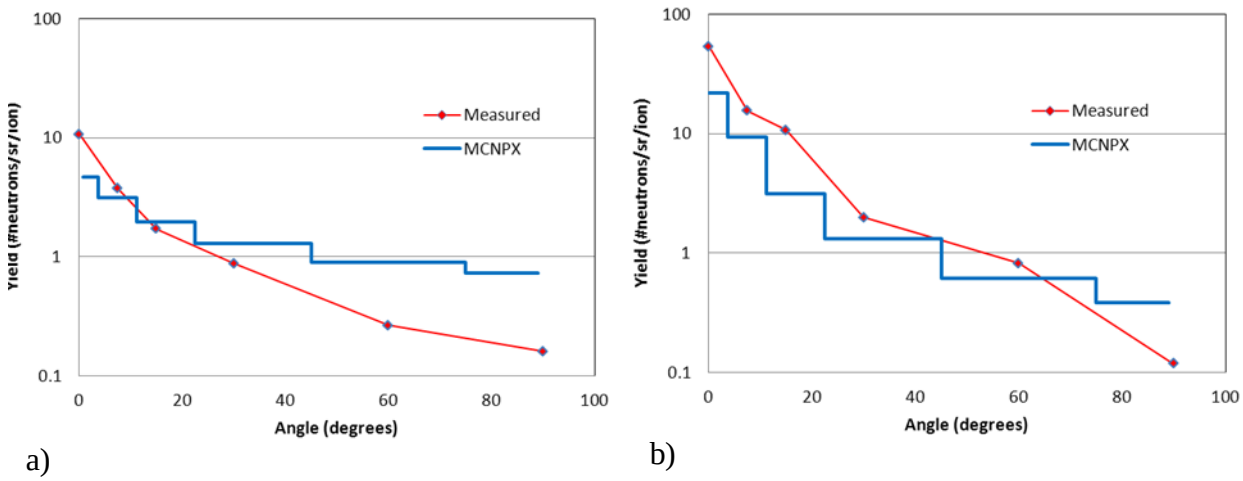

FIG. 15—*Measured and calculated angular distribution of neutrons from a) 400 MeV/nucleon C on 5.0-cm-thick Cu target, and b) 400 MeV/nucleon Ar on 5.5-cm-thick Al target. Simulations were performed with the MCNPX code.*